J. Am. Ceram. Soc., 95 [10] 3325–3333 (2012)
DOI: 10.1111/j.1551-2916.2012.05350.x

journal

Synthetic Coal Slag Infiltration into Varying Refractory Materials

Tetsuya K. Kaneko,[‡,§,†] Hugh Thomas,[¶] James P. Bennett,[¶] and Seetharaman Sridhar[‡,§]

[‡]US Department of Energy, National Energy Technology Laboratory, 626 Cochrans Mill Road, Pittsburgh, Pennsylvania 15236

[§]Department of Materials Science and Engineering, Carnegie Mellon University, 5000 Forbes Avenue, Pittsburgh, Pennsylvania 15213

[¶]US Department of Energy, National Energy Technology Laboratory, 1450 Queen Avenue, Albany, Oregon 97321

The infiltrations of synthetic coal slag into 99%Al_2O_3, 85% Al_2O_3–15%SiO_2, and 90%Cr_2O_3–10%Al_2O_3 refractories with a temperature gradient induced along the penetration direction were compared to one another. The infiltrating slag was synthesized with a composition that is representative of an average of the ash contents from U S coal feedstock. Experiments were conducted with a hot-face temperature of 1450°C in a CO/CO_2 atmosphere. Minimal penetration was observed in the 90%Cr_2O_3–10%Al_2O_3 material because interactions between the refractory and the slag produced a protective layer of $FeCr_2O_4$, which impeded slag flow into the bulk of the refractory. After 5 h, the 99%Al_2O_3 sample exhibited an average penetration of 12.7 mm whereas the 85%Al_2O_3–15%SiO_2 sample showed 3.8 mm. Slag infiltrated into the 99%Al_2O_3 and 85%Al_2O_3–15%SiO_2 refractory systems by dissolving the respective refractories' matrix materials, which consist of fine Al_2O_3 particles and an amorphous alumino-silicate phase. Due to enrichment in SiO_2, a network-former, infiltration into the 85%Al_2O_3–15%SiO_2 system yielded a higher viscosity slag and hence, a shallower penetration depth. The results suggest that slag infiltration can be limited by interactions with the refractory through the formation of either a solid layer that physically impedes fluid flow or a more viscous slag that retards infiltration.

I. Introduction

Among various energy generation technologies, entrained-flow gasification offers the potential to simultaneously convert mixtures of carbon-based materials such as coal, biomass, and petroleum coke into a fuel rich in CO and H_2 gases. The ability to utilize a wide breadth of carbon feedstock options provides increased flexibility and greater reductions in CO_2 emissions. However, with temperatures and pressures as high as 1575°C and 2.8 MPa, materials stability issues hinder the commercial viability of gasification systems.[1] As a consequence of the elevated temperatures, the mineral impurities from the feedstock fuse together and attack the porous refractory lining that protects the external shell of the gasifer. Once the slag infiltrates into the refractory, changes in the chemical and physical properties of the materials result in crack and void formation from near the refractory surface to the point of slag infiltration.[2,3]

Factors that influence the penetration of molten slag into refractory include temperature, gasification atmosphere, refractory porosity, slag composition, and interfacial surface properties of the slag with respect to microstructure and chemistry of the refractory material.[4–10] This analysis focuses upon understanding the role that refractory composition and microstructure has on slag infiltration resistance against synthetic coal slag. A synthetic oxide mixture with a chemistry simulating an average of the U S coal ash contents was infiltrated into three commercially available refractories with varying chemical compositions. The compositions of the examined refractories were predominately comprised of Al_2O_3, Al_2O_3–SiO_2, and Cr_2O_3–Al_2O_3. The selection of the refractories was based upon their potential to exhibit a spectrum of phenomena that would limit infiltration. The infiltrated refractory samples were studied using microscopy and diffraction techniques to identify product phases, changes in morphology, and evolution in chemical composition of the slag as a function of penetration depth.

II. Materials and Methods

(1) Materials

Synthetic slag with a composition resembling the mineral impurity constitution of coal feedstock in an entrained-flow slagging gasifier was used in this investigation. A representative slag composition[11] was produced by taking an averaging of ash constituents derived from sub-bituminous coal feedstock in the United States.

Chemically pure oxide powders were weighed and mixed to their appropriate ratios, then melted in a high-density Al_2O_3 crucible at 1450°C in a CO/CO_2 gas mixture with a ratio of 1.8, corresponding to an oxygen partial pressure of 10^{-8} atm. The slag was cooled at roughly 20°C/min by lowering the sample and the surrounding Al_2O_3 furnace tube out of the hot-zone. Upon extracting the vitreous material from the crucible, it was ground into roughly 2 mm particles. The slag compositions were analyzed using inductively coupled plasma mass spectrometry (ICP-MC). The desired target composition and the experimentally realized compositions are summarized in Table I.

Commercial 99%Al_2O_3, 85%Al_2O_3–15%SiO_2, and 90% Cr_2O_3–10%Al_2O_3 refractory bricks were machined into cylindrical cups for accepting the slag. Detailed compositions of the refractory materials are summarized in Table II. The outer dimensions of the samples were machined to a diameter of 5.08 cm and a height of 11.11 cm. The cup portions of the samples were machined to a diameter of 3.18 cm and a height of 3.49 cm.

(2) Experimental Methods

To verify the constituents and characteristics of the starting materials, the synthetic slag and the refractories in their virgin states were examined using a FEI Quanta 600 (FEI, Hillsboro, OR) environmental scanning electron (ESEM) microscope with energy dispersive spectroscopy (EDS),

M. Rigaud—contributing editor

Manuscript No. 31170. Received March 07, 2012; approved June 04, 2012.
[†]Author to whom correspondence should be addressed. e-mail: tkaneko@andrew.cmu.edu

Table I. Target Composition and Experimentally Achieved Compositions of Synthetic Coal Slag. Results are Presented in at.%

	Al_2O_3	SiO_2	FeO	CaO	MgO	Na_2O	K_2O
Target	18.30	53.70	15.90	7.67	2.31	1.02	1.1
CO/CO_2	19.07	53.08	15.19	7.79	2.13	0.82	1.90

Table II. Compositions of Refractory Materials. Results are Presented in at.%

	Al_2O_3	SiO_2	Cr_2O_3	CaO	MgO	Fe_2O_3	Na_2O
99%Al_2O_3	99.62	0.03	0	0	0	0.01	0.33
85%Al_2O_3–15%SiO_2	84.79	14.86	0	0.17	0	0.18	0
90%Cr_2O_3–10%Al_2O_3	9.87	0.05	89.65	0.21	0.13	0.09	0

secondary-electron (SE), and back-scattered electron (BSE) imaging. The porosity and average pore size of the refractories were measured using a Micromeritic AutoPore IV 9500 Series mercury porosimeter (Norcross, GA). Both the starting slag and the refractory materials were individually pulverized and scanned using a PANalytical (Almelo, the Netherlands) X-ray diffraction (XRD) system with a PIXcel 1D line detector. A step size of 0.025° and an effective time per step of 2000 s. were used. The effective time per step refers to the time it would take an 0D detector system to complete the same single step. A variable slit configuration with a 10 mm mask was used and the symmetrical scan ranged from 20° to 70°.

A vertical tube furnace, manufactured by Lindberg, was used to thermally treat the slag and refractory materials. Experiments were conducted with a temperature gradient induced along the penetration direction of the sample by deliberately stepping the lower portions of the sample below the hot-zone of the furnace. The temperature gradient was designed to emphasize the native temperature gradients that are present in actual gasifiers due to differential heating conditions at the hot face and the cold face of the refractory lining. Refractories in actual gasifiers typically experience 100°C or greater drops in temperature at roughly 50 mm depths from the working hot-face. The thermal profile, shown in Fig. 1, was experimentally verified by probing a refractory sample with thermocouples along its length at 25.4 mm intervals. Once the refractory sample achieved the desired thermal profile, 40 g of granulated slag was inserted into the top of the furnace through a quartz tube. An illustration of the deposition process is shown in Fig. 2. The experiments were conducted in the same CO/CO_2 atmosphere used for melting the slag. The objective of the experiments was to simulate conditions that are similar to those encountered in entrained-flow gasifiers, which typically operate at oxygen partial pressures between 10^{-9} and 10^{-7} atm. The slag was deposited onto the refractory at temperature rather than placed there before the heating cycle to ensure that slag would not infiltrate into the refractory before the proper experimental conditions were met. The furnace was immediately resealed after the deposition. After holding the experiment for 5 h, the refractory sample was cooled at roughly 15°C/min in the same way as the slag sample was cooled. The sample was not rapidly quenched to room temperature because that could induce micro-cracks and damage the microstructure of the sample.

The samples were cross-sectioned to expose the infiltration of the slag into the refractory and progressively polished to a 0.5 μm finish using a Struers TegraPol-25 polisher (Copenhagen, Denmark). Polished samples were examined using ESEM for morphological observations and chemical analyses. Small quantities of the samples were pulverized and analyzed using XRD to examine the crystalline phases. XRD scan parameters identical to those for the starting materials were used.

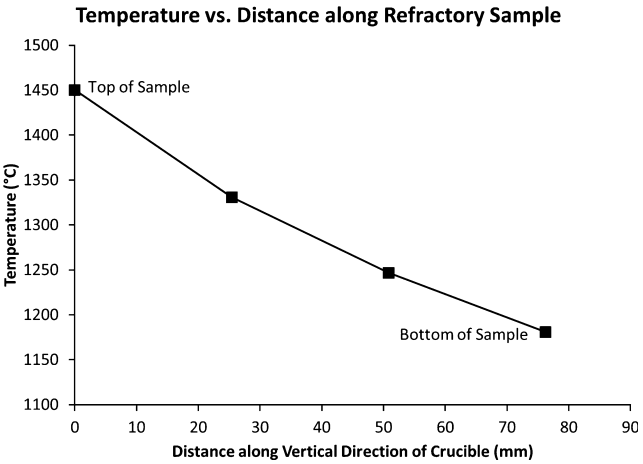

Fig. 1. Plot of the temperature gradient induced along the penetration direction of the refractory sample.

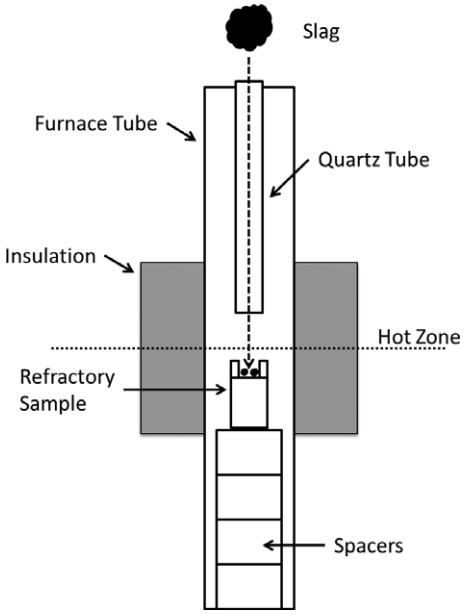

Fig. 2. Illustration of experimental set-up during the deposition of the ash onto the refractory sample.

(3) Physical Model

Open pores and micro-cracks are the main channels for slag to penetrate into the refractory. Assuming that the pores are adequately networked, the slag flows in an omnidirectional manner through cylindrical tubes of similar cross-sections. The temperature gradient present along the penetration direction induces a viscosity and density gradient in the slag fluid. The viscosity[12,13] of the slag can range from 0.1 to 100 Pa·s as a response to the temperature gradient. The density of the slag, on the other hand, remains relatively stable throughout the temperature gradient. For slags with similar compositions as those studied in this analysis, the density[14] ranges from 3500 to 3800 kg/m^3 within the considered temperatures. The slag fluid can therefore be considered incompressible, but capable of demonstrating a wide range of dynamic viscosities. The average pore radius is on the scale of micrometers, while the penetration length is on the scale of millimeters or greater. When slag flows into the

pores, the slag passes through vertical capillaries with radius R, and length L. By applying a lubrication approximation on the basis that $R/L \ll 1$, the terms associated with convection and variable viscosity vanish. The change in viscosity induced by the temperature gradient is enveloped in an effective viscosity term, which is unique to the conditions that alter the thermo-physical properties of the fluid. With the assumption that capillary pressures drive the slag fluid into the pores, the momentum equation simplifies as follows:

$$\frac{\mathrm{d}l}{\mathrm{d}t} = \frac{r\gamma\cos(\theta)}{4\int_0^{l(t)}\eta(z)\mathrm{d}z} \tag{1}$$

where r is the pore radius, γ is the surface tension of the slag, θ is the contact angle of the slag with the pore wall, η is the dynamic viscosity of the slag, and l is the penetration depth of the slag that is perpendicular to the slag/refractory interface. This relationship elucidates that slag penetration can be suppressed by increasing the slag viscosity and contact angle, or by decreasing the surface tension. Using Eq. (1), penetration depths were calculated using the following methodology:

1. Slag compositions from the penetration front of the experimental samples were extracted using ESEM-EDS.
2. Slag viscosities were calculated using an appropriate viscosity model with respect to the slag composition extracted in step 1 and the range of temperatures observed in the temperature gradient. Since a static composition was used for each calculation, slag viscosity was reduced to a function of temperature, $\eta(T)$.
3. The experimentally measured thermal profile was used to express temperature as a function of penetration depth, $T(l)$. A polynomial equation was fitted to slag viscosity to describe it in terms of penetration depth, $\eta(l)$.
4. The viscosity relation developed in step 3, $\eta(l)$, was substituted into Eq. (1) to project the penetration depth of the slag with respect to elapsed time.

III. Results

(1) Characterization of Starting Materials

Microscopy of the starting synthetic coal slag did not resolve any distinct features that belong to crystalline phases. XRD powder scan of the material confirmed this observation with low intensities and the lack of peaks. ESEM micrographs of the refractories in their virgin states are shown in Fig. 3. All three refractory materials were comprised of two structurally distinct regions. Dispersed throughout the refractory were dense aggregates. The surrounding regions constituted the matrix, where finer particles sinter together and act as the bonds between the larger aggregates.

The 99%Al_2O_3 and 85%Al_2O_3–15%SiO_2 systems contained tabular aggregates with chemistries resembling the respective bulk compositions. The aggregates from these systems demonstrated a greater degree of closed porosity as compared to the fused aggregates from the 90%Cr_2O_3–10%Al_2O_3 system. The BSE micrograph of the 90%Cr_2O_3–10%Al_2O_3 system in Fig. 3(c) illustrates that variations in composition were present in the aggregate materials. The brightly contrasted regions contained higher concentrations of the Cr_2O_3 whereas the darkly contrasted regions contained higher concentrations of Al_2O_3.

The microstructures of matrix regions belonging to the 99%Al_2O_3 and 90%Cr_2O_3–10%Al_2O_3 systems consisted of fine particles with thin layers of a glassy alumino-silicate phase designed to assist in the sintering behavior between the aggregate and matrix particles. The bonding phase of the 90%Cr_2O_3–10%Al_2O_3 systems is shown in Fig. 4. The chemistries of the fine matrix particles also resembled the

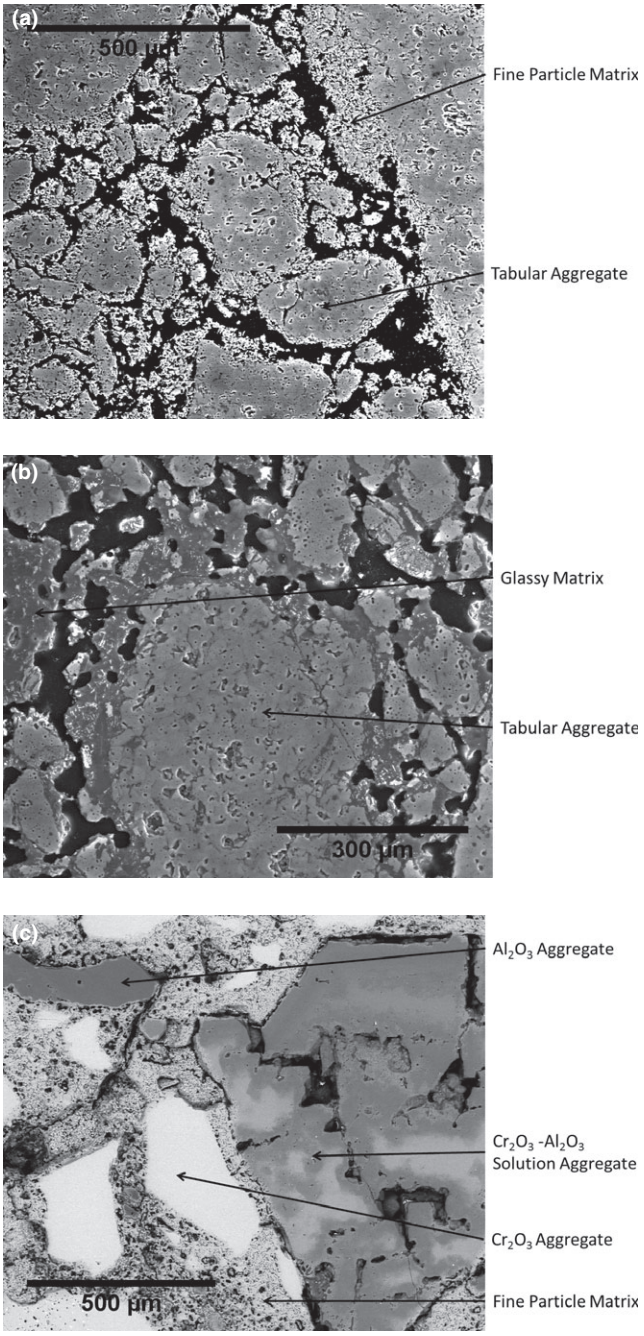

Fig. 3. ESEM micrographs of virgin (a) 99%Al_2O_3, (b) 85%Al_2O_3–15%SiO_2, and (c) 90%Cr_2O_3–10%Al_2O_3 refractory microstructures.

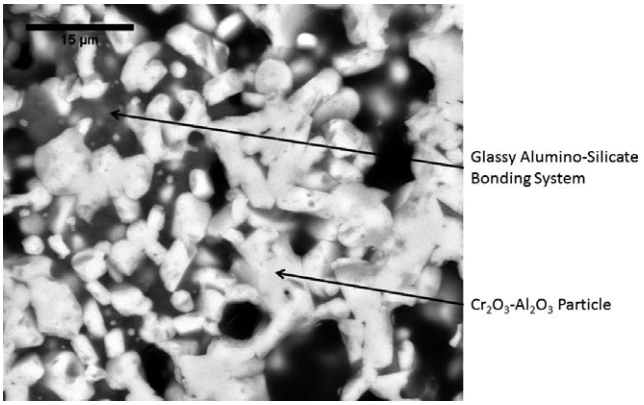

Fig. 4. ESEM micrograph of matrix region belonging to 90%Cr_2O_3–10%Al_2O_3 system.

respective bulk compositions of the refractory materials. Alternatively, the matrix region of the 85%Al_2O_3–15%SiO_2 system was nearly devoid of the fine particles, and largely consisted of the glassy bonding phase. As a result of the lack of fine particles to fill in the matrix regions, voids formed around the aggregates. High-aspect ratio mullite ($Al_6Si_2O_{13}$) grains were suspended within the glassy matrix phase of the 85%Al_2O_3–15%SiO_2 system.

XRD powder scans of the virgin refractories are displayed in Fig. 5. The scan for the 99%Al_2O_3 refractory system shows peaks belonging solely to the corundum structure Al_2O_3 phase. The scan for the 85%Al_2O_3–15%SiO_2 system reveals peaks corresponding to the corundum structure Al_2O_3 parent material along with the $Al_6Si_2O_{13}$ crystals suspended within the glassy bonding phase. The scan of the 90%Cr_2O_3–10%Al_2O_3 system shows peaks attributable to a corundum structure Cr_2O_3–Al_2O_3 solid solution phase[15] with two noticeably different lattice parameters. The variation in solution chemistry is especially apparent at the higher 2θ angles where the respective phases' peaks separated from one another.

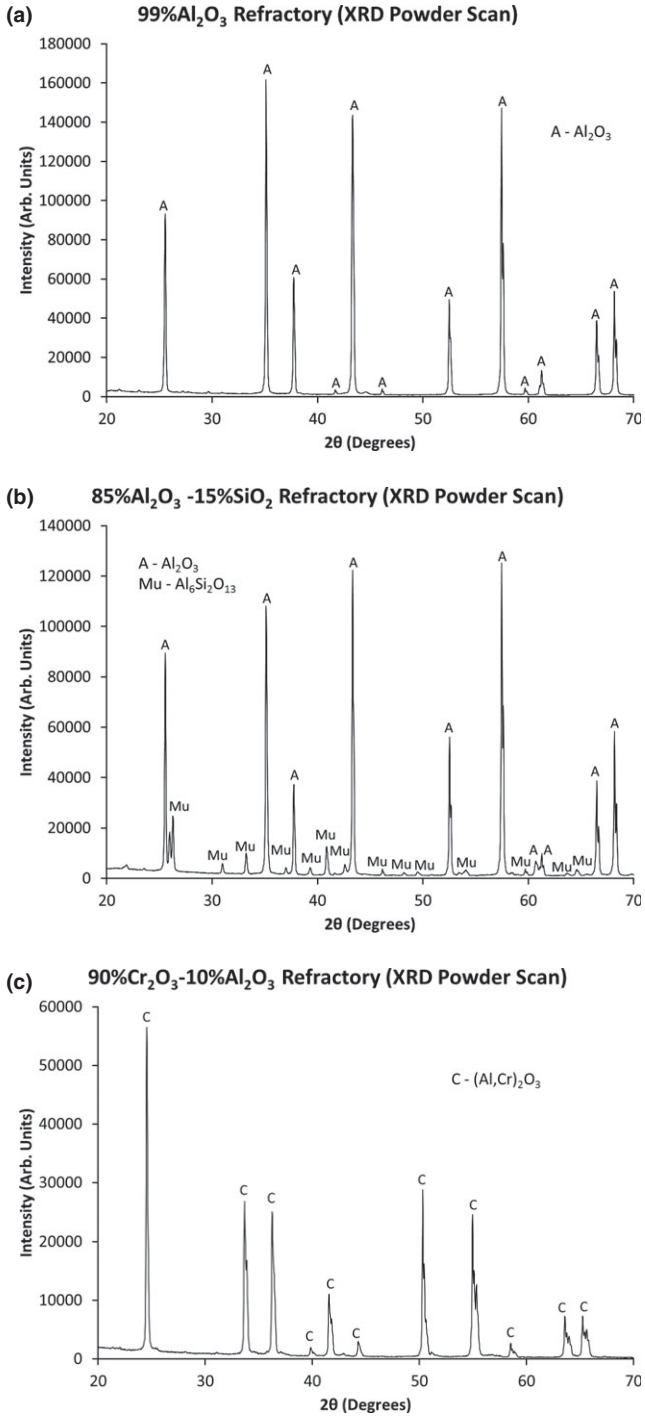

Fig. 5. XRD powder scans of (a) 99%Al_2O_3, (b) 85%Al_2O_3–15%SiO_2, and (c) 90%Cr_2O_3–10%Al_2O_3 refractory materials before infiltration.

The plot in Fig. 6 shows that although varying in both size and frequency, two distinct pore size distributions were present in the refractories. The larger pores correspond to pores constructed by the voids between the particles in the matrix region. The smaller pores correspond to the porosity originating from within the aggregates and the particulates. The 85%Al_2O_3–15%SiO_2 system demonstrates the greatest distinction between the two pore varieties because the absence of fine particles in the matrix region resulted in voids that were significantly larger than the closed porosity of the aggregates. The 99%Al_2O_3, 85%Al_2O_3–15%SiO_2, 90%Cr_2O_3–10%Al_2O_3 refractory systems, respectively, demonstrated mean pore radii of 0.92, 3.62, and 1.47 μm.

(2) Macroscopic Infiltration Trends

Photographs of the cross-sectioned infiltrated refractories are shown in Fig. 7. The penetration depths were measured as the distance to which the slag was observed to have macroscopically infiltrated into the base of the refractory samples. Over the 5 h experimental duration, the synthetic coal slag infiltrated 12.7 mm into the 99%Al_2O_3 and 3.1 mm into the 85%Al_2O_3–15%SiO_2 refractories. Macroscopically, the 90% Cr_2O_3–10%Al_2O_3 refractory showed minimal signs of penetration by the synthetic coal slag material. In all three cases, slag that had not penetrated into the refractories cooled as glassy slag reservoirs at the top of the refractory samples. The slag reservoir of the 90%Cr_2O_3–10%Al_2O_3 material appears irregularly shaped because parts of the reservoir fractured during sample preparation. Prior to the fracturing, the slag reservoir appeared similarly to the others.

(3) Slag Infiltration and Phase Formation

Whereas the 90%Cr_2O_3–10%Al_2O_3 refractory effectively blocked slag penetration, the 99%Al_2O_3 and 85%Al_2O_3–15%SiO_2 refractories permitted varying degrees of slag infiltration through the matrix regions of the refractory microstructure. As illustrated by the BSE micrograph in Fig. 8(a), a reaction phase produced by the interactions between the refractory and slag materials uniformly coated the top interface of the infiltrated 90%Cr_2O_3–10%Al_2O_3 sample,

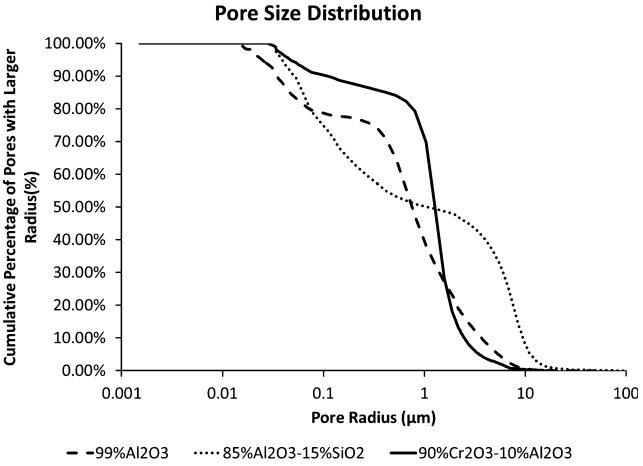

Fig. 6. Pore size distributions of the refractory systems. The plot indicates that the refractories' respective microstructures significantly impact the available pathways for the infiltrating slag.

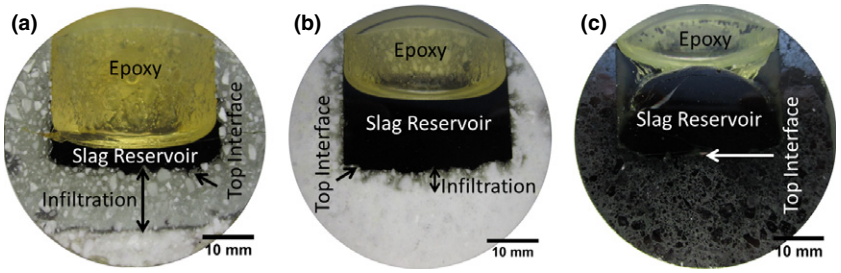

Fig. 7. Photographs of infiltrated samples. (a) 99%Al_2O_3 sample experiences the deepest penetration with 12.7 mm. (b) 85%Al_2O_3–15%SiO_2 sample demonstrates 3.85 mm of penetration. (c) 90%Cr_2O_3–10%Al_2O_3 sample shows no macroscopically visible penetration.

effectively forming a barrier. The product layer spanned the entire top interface and was roughly 31 μm thick. EDS analysis indicated that the product phase was chromite ($FeCr_2O_4$). The XRD powder scan of the infiltrated refractory in Fig. 11 confirms the presence of $FeCr_2O_4$ alongside the background associated with the Cr_2O_3–Al_2O_3 corundum solid solution phase of the refractory. Depending on whether the slag reacted with the surfaces of the coarse aggregates or the granular and porous matrix regions, the morphology of $FeCr_2O_4$ layer varied. When it formed at the interface between the slag and the aggregate grains, the cross-section of $FeCr_2O_4$ layer was smooth with very few pits and voids. However, when it formed at the interface between the slag and the matrix regions, the $FeCr_2O_4$ layer consisted of many fragmented $FeCr_2O_4$ grains, which resembled the shape and size of the underlying refractory material. Irrespective of how and where the product phase formed, the $FeCr_2O_4$ layer served to plug any entryways into the bulk of the refractory. Figure 8(b), the EDS map of the same region pictured in Fig. 8(a) illustrates how the $FeCr_2O_4$ layer prohibited the flow of slag fluid into the refractory through either aggregate or matrix regions. The Si map, which is associated with the slag for its having a higher SiO_2 content, demonstrates that negligible volumes of slag passed through the $FeCr_2O_4$ layer.

As demonstrated by the ESEM micrographs of the infiltrated samples in Figs. 9 and 10, the slag preferentially penetrated through the porous matrix regions of the refractory microstructure. Although the structural and compositional natures of the matrix materials were significantly different from

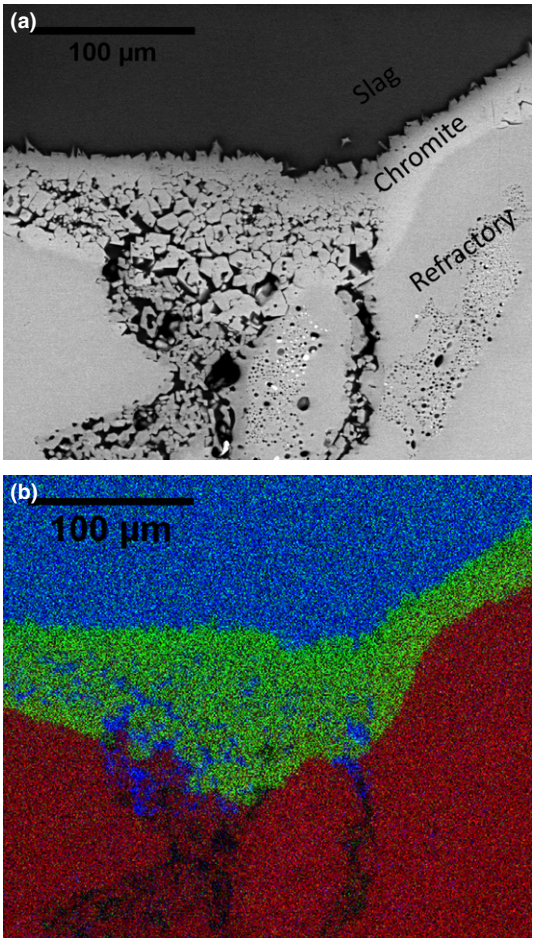

Fig. 8. (a) BSE micrograph of top interface of 90%Cr_2O_3–10%Al_2O_3 sample. A chromite ($FeCr_2O_4$) layer protects the refractory from the slag penetration. (b) Accompanying EDS map with blue, green, and red areas, respectively, associated with Si, Fe, and Cr species.

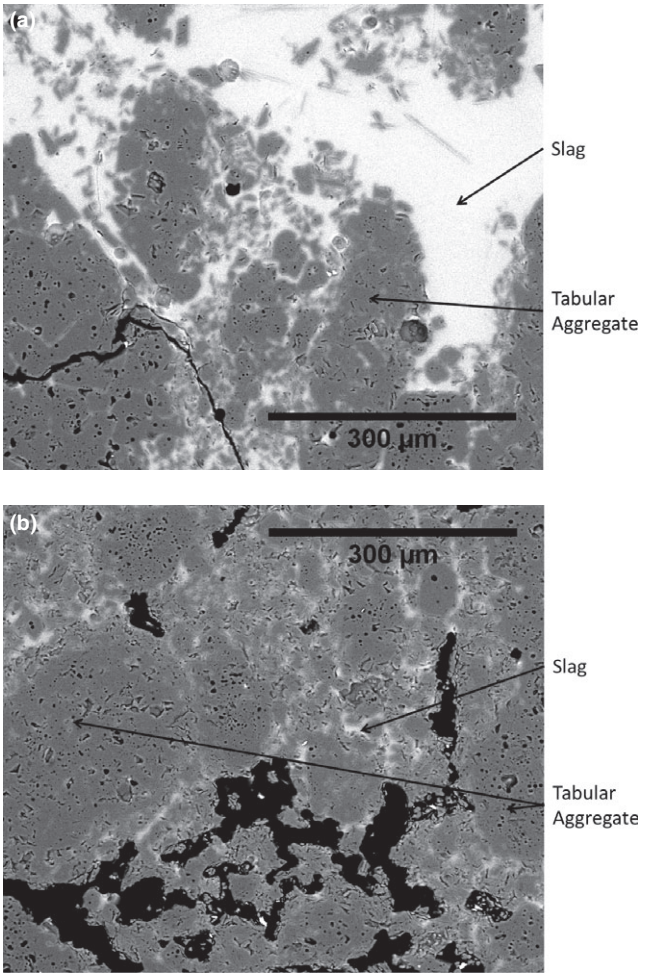

Fig. 9. (a) Top and (b) bottom interfaces of infiltration into 99%Al_2O_3 sample. The fine particle matrix microstructure gradually becomes coherent closer to the penetration front.

one another, the slag persisted to consume the porous regions to leave behind a trail of suspended aggregate grains near the top interfaces of the samples. At the penetration front, the microstructure belonging to the matrix region of the 99% Al_2O_3 system gradually transitioned back to that of the virgin refractory. The extent of dissolution by the slag subsided, so the fine Al_2O_3 particles remained packed between the dense aggregate grains. In contrast, the matrix microstructure of the 85%Al_2O_3–15%SiO_2 system experienced an abrupt shift at the penetration front. A sharp transition in the wetting characteristics of the slag and the glassy alumino-silicate bonding phase with respect to the refractory grains distinctly marked the penetrated and virgin regions. Although the glassy bonding phase only partially wetted the refractory grains, the incoming slag entirely enveloped them.

Fine $Al_6Si_2O_{13}$ grains, comparable in shape and size to the ones embedded within the glassy bonding phase of the virgin matrix region, were suspended in the infiltrated pores of the 85%Al_2O_3–15%SiO_2 refractory. The XRD powder scan of the infiltrated region of the 85%Al_2O_3–15%SiO_2 refractory in Fig. 11 displays peaks with nearly identical relative intensities and positions as the XRD scan of the virgin refractory material in Fig. 5. The similarities in XRD powder scans and $Al_6Si_2O_{13}$ grains morphologies between the infiltrated and virgin samples suggest that the $Al_6Si_2O_{13}$ in the infiltrated pores likely originated from the starting refractory material. ESEM as well as XRD powder scan of the infiltrated 99%Al_2O_3 sample did not resolve any phases that may have formed as a result of solidification or reactions between the refractory and slag materials.

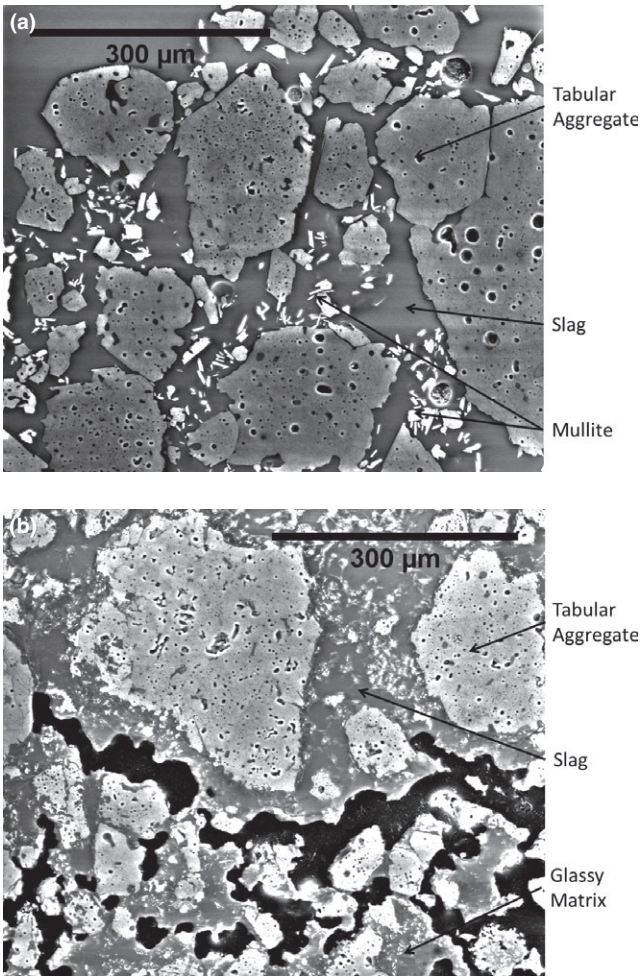

Fig. 10. (a) Top and (b) bottom interfaces of infiltration into 85% Al_2O_3–15%SiO_2 sample. The infiltrating slag aggressively attacks the glassy bonding matrix phase until the very end of the penetration.

(4) Slag Composition Within the Refractory Pores

Figure 12 plots the composition profiles of the slag constituents with respect to the penetration depth for the 99%Al_2O_3 and 85%Al_2O_3–15%SiO_2 refractory systems. For infiltration into the 90%Cr_2O_3–10%Al_2O_3 refractory, changes in slag composition were not recorded because the $FeCr_2O_4$ layer that formed on the top interface of the refractory effectively obstructed the slag from proceeding into the bulk material. Slag that infiltrated into the 99%Al_2O_3 refractory system experienced an increase in Al_2O_3 concentration. Slag that was deposited onto 85%Al_2O_3–15%SiO_2 refractory system experienced a significant increase in SiO_2 concentration as compared to the other slag constituents. For both experimental cases, composition gradients developed based on the respective oxide species increasing with penetration depth.

IV. Discussion

From the observations made in the results section, the following points can be summarized with respect to the synthetic coal slag infiltrations into the different refractory systems:

1. Formation of a substantially thick layer of chromite ($FeCr_2O_4$) on the top interface obstructed slag infiltration into the 90%Cr_2O_3–10%Al_2O_3 refractory.
2. Slag preferentially attacked and infiltrated through the porous matrix regions of the 99%Al_2O_3 and 85%Al_2O_3–15%SiO_2 refractory systems.
3. Rapid dissolution of the predominantly glassy matrix phase of 85%Al_2O_3–15%SiO_2 material by the slag

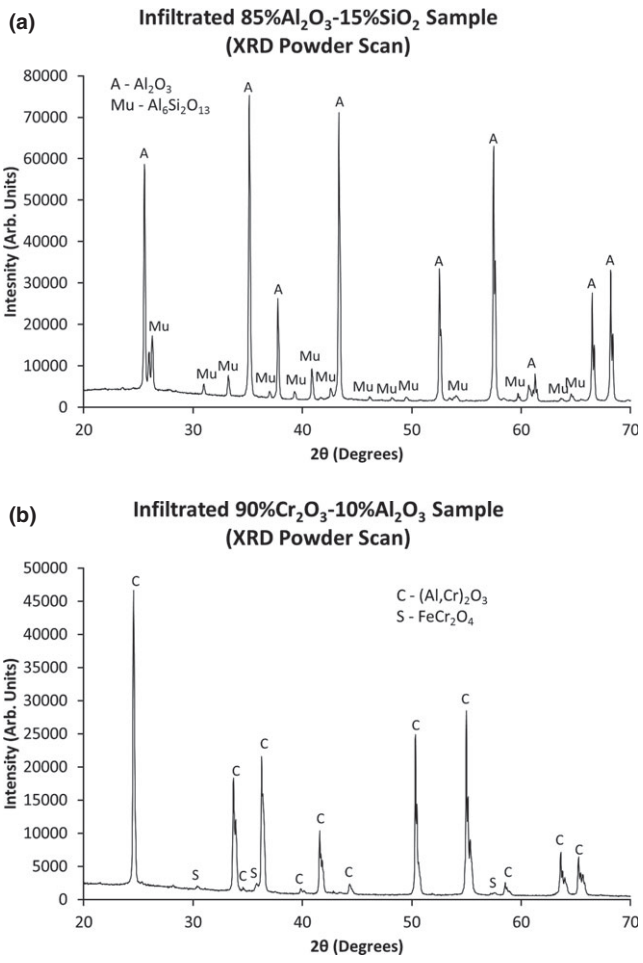

Fig. 11. XRD powder scans of infiltrated (a) 85%Al_2O_3–15%SiO_2 and (b) 90%Cr_2O_3–10%Al_2O_3 samples.

resulted in an abrupt microstructural transition from the infiltrated to virgin regions.

4. Extensive dissolution of SiO_2, a network-forming species, from the 85%Al_2O_3–15%SiO_2 material yielded a high viscosity slag and helped limit slag penetration.

The liquid-solid reactions at the top interface between the slag and 90%Cr_2O_3–10%Al_2O_3 refractory prevented slag from infiltrating into the refractory microstructure. The thick layers of $FeCr_2O_4$ functioned as barriers to not only block fluid flow into the bulk refractory, but also to reduce corrosion by instituting an indirect dissolution path between the slag and the virgin refractory material. Although the 90%Cr_2O_3–10%Al_2O_3 refractory formed a substantial barrier layer in response to the coal slag, the 99%Al_2O_3 and 85%Al_2O_3–15%SiO_2 refractories failed to construct a comparable physical obstacle to mitigate infiltration. Pseudo-binary phase diagrams, which simulate the synthetic slag in contact with the respective refractory systems, are shown in Fig. 13. Diffusion paths for multi-component systems that contain species with varying diffusivities rarely exhibit direct trajectories in the respective phase fields. The diagrams generated using FactSage[16] 6.2 in Fig. 13 are thus simplifications to represent some of the phases that may appear, assuming that the species behave similarly to one another with regard to diffusion. With the starting slag composition on the left and the refractory compositions on the right, the diagrams qualitatively depict the phases that would appear if the system from the center of the pore to the pore wall were to be viewed as a diffusion couple. The pore wall is assumed in be in local equilibrium with the infiltrating slag. The calculations consider mullite structures, corundum structures, spinel structures, and slag as possible phases that could form in the system. To represent the synthetic slag, the SlagA solution phase was selected since it is optimized for many of the major oxide components in the slag. Similarly, to represent the refractory materials, the Corundum solution phase was selected. Mullite and Spinel solution phases were selected to describe mullite and spinel structures that could form with the active species. Oxide species of SiO_2, Al_2O_3, FeO, Cr_2O_3, MgO, and CaO were considered in the calculations.

FactSage predictions agreed with the experimental infiltration results for the 90%Cr_2O_3–10%Al_2O_3 system and showed

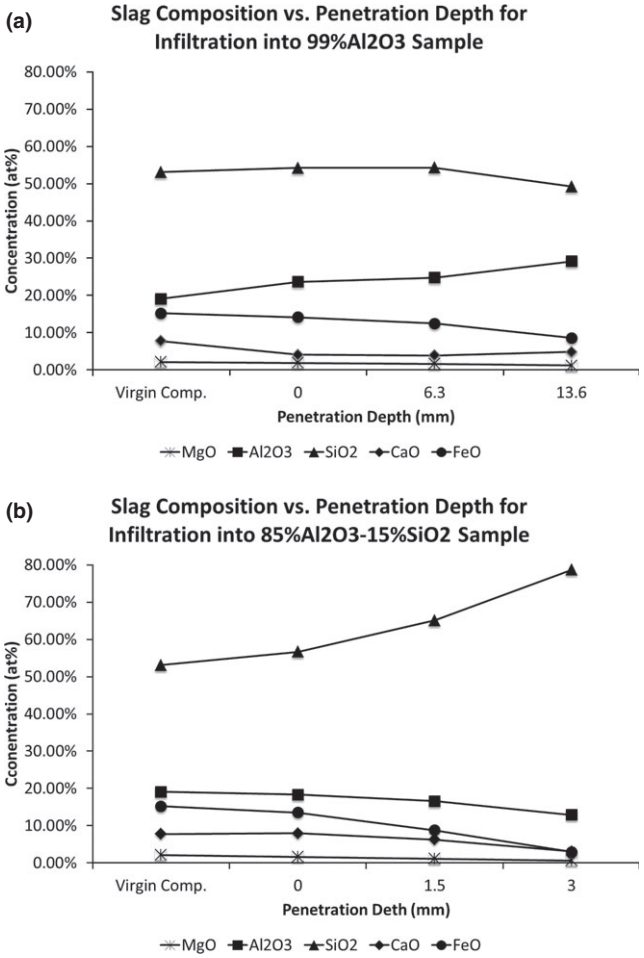

Fig. 12. Slag composition with respect to penetration depth for infiltration into (a) 99%Al_2O_3 and (b) 85%Al_2O_3–15%SiO_2 refractories.

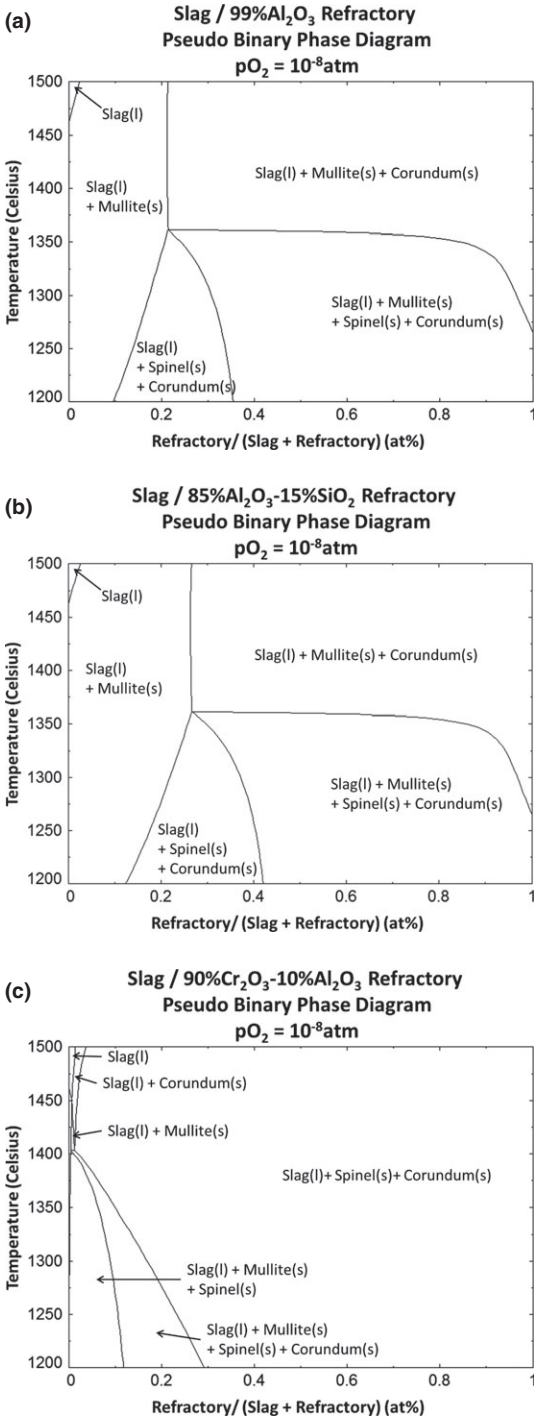

Fig. 13. Pseudo-binary phase diagrams simulating synthetic coal slag in contact with (a) 99%Al_2O_3, (b) 85%Al_2O_3–15%SiO_2, and (c) 90%Cr_2O_3–10%Al_2O_3 refractories.

that slag, refractory, and spinel should be in equilibrium with one another. Due to equilibrium constraints between the slag and the refractory, $FeCr_2O_4$ demonstrated the greatest solid solution chemistry among the other isomorphic spinel species. For infiltrations into the 99%Al_2O_3 and 85%Al_2O_3–15%SiO_2 systems, FactSage predicted that slag, refractory, and mullite should be in equilibrium with one another. The experimental results in Figs. 9 and 10 show that while infiltration into the 85%Al_2O_3–15%SiO_2 system produced mullite, infiltration into the 99%Al_2O_3 system did not produce additional volumes of mullite. Mullite ($Al_6Si_2O_{13}$) was not resolved even at the slag/refractory interface, where the pseudo-binary phase diagrams are most relevant. The phase diagrams can only project that $Al_6Si_2O_{13}$ should be present, but due to the metastable nature of slags and melts, they cannot estimate definitive time scales or volumetric amounts at which the phases may form.

Figure 13 indicates that $FeCr_2O_4$ spinel should form at the slag/refractory interface for the 90%Cr_2O_3–10%Al_2O_3 refractory and $Al_6Si_2O_{13}$ for the 99%Al_2O_3 and 85%Al_2O_3–15%SiO_2 refractories. The latter was not experimentally observed. This discrepancy between thermodynamic prediction and experimental observation is most easily attributable to the possibility that the diffusion paths taken by the experimental system were not visualized in the phase diagrams. As mentioned earlier, diffusion paths for multi-component systems that contain species with varying diffusivities rarely demonstrate direct trajectories as represented by pseudo-binary phase diagrams. However, if the diagrams in fact represented the appropriate diffusion paths, then the relative diffusivities of the cation species could have limited the formation of the mixed oxide solids. Since the refractory microstructure offered an abundance of heterogeneous nucleation sites, the product phases of interest can be assumed to have nucleated with sufficient driving force. The growth process of the crystalline phase may have limited the system from forming the equilibrium phases on the resolvable scale. The temperature and the diffusivity of the species involved in the process determine the growth rate of solids. Since the samples were exposed to identical temperatures, the diffusivity of the species can be regarded as the limiting term. In oxide melts with ratios between SiO_2 and Me_xO that are comparable to the ratio of the synthetic slag of this study, the Si cation diffuses roughly three orders of magnitude slower than Fe cation.[14,17,18] The substantially lower diffusivity of the Si cation in the slag could have hindered $Al_6Si_2O_{13}$ crystals from not only forming a dense barrier layer against slag flow, but also growing into resolvable sizes with either ESEM or XRD.

With the 99%Al_2O_3 system, the slag preferentially consumed the fine Al_2O_3 particles belonging to the matrix regions since they possessed greater surface area to volume ratios than their aggregate counterparts. Furthermore, the fine particles were coated with thin layers of a glassy alumino-silicate material, which lowers the local melting temperatures and encourages further dissolution into the slag. The dissolution process was greatest near the top interface and decreased as the slag progressed deeper into the bulk refractory. This behavior is attributable to the chemistry of the slag as well as the temperature gradient induced through the refractory. Upon contacting the refractory, the driving force of the slag to dissolve the matrix material decreased with time and depth since the local chemistries within the pores progressed to compositions that were closer to equilibrium. To strengthen this process, the higher temperatures closer to the top interface provided greater thermal energies to propel the transport phenomena that govern dissolution. As the slag progressed into the deeper regions of penetration, the refractory microstructure was impacted less by chemical dissolution by the slag.

With the 85%Al_2O_3–15%SiO_2 system, the synthetic coal slag favorably consumed the glassy bonding phase. The matrix regions largely consisted of the glassy phase so additional kinetic processes controlling phase transformations of crystalline solids into ionic liquid were bypassed. Since the glassy bonding phase integrated into the slag quicker than the fine refractory particles, a very sudden microstructural transition was observed at the interface where the fluid head and the virgin refractory met.

The change in the composition of the slag with respect to the starting slag composition was heavily dependent on the interactions with the uniquely different compositions and morphologies of the matrix materials of the 99%Al_2O_3 and 85%Al_2O_3–15%SiO_2 refractories. As noted, the matrix of the 99%Al_2O_3 system contained fine Al_2O_3 particles that were held together by small quantities of glassy alumino-silicate material. The matrix of the 85%Al_2O_3–15%SiO_2 system primarily consisted of the glassy alumino-silicate phase, which exhibited high concentrations of SiO_2. Figures 9 and 10 demonstrate that the slag interacted with the respective matrix regions by means of consuming the materials. The plots in Fig. 12, which track slag chemistry with respect to penetration depth, correspond to these microstructural observations and show that the Al_2O_3 and SiO_2 concentrations of the slag increased, respectively, when infiltrating into the 99%Al_2O_3 and 85%Al_2O_3–15%SiO_2 systems. The compositions at the fluid heads demonstrated the greatest deviations from the starting slag composition for their being the first bodies of fluid to enter the refractory. The fluid head was permitted the longest periods of time to interact with virgin refractory material and incur chemical changes. For the same reason, slag near the top interface exhibited lesser deviations in concentration because it was given shorter times to interact with the refractory. Composition profiles developed where the concentration of either Al_2O_3 or SiO_2 increased from the top interface to where the infiltration terminated. With enrichment in SiO_2, the slag in the 85%Al_2O_3–15%SiO_2 system turned significantly more viscous and thereby assisted in limiting the effective slag penetration depth into the refractory.

Equation (1) was used to evaluate how refractory composition and microstructure impacted infiltration. Considering that the conditions at the fluid head are most pertinent in determining slag penetration depths, chemical constitutions were extracted from the very ends of the experimental infiltrations and used to fulfill the numerical model. Reactive systems, with slag wetting mixed oxide materials, can have contact angles that vary over the course of minutes.[19] A delay in experimental time is inevitable for surface properties to stabilize because equilibrium is reached through chemical and physical changes induced by phenomena such as dissolution and formation of new phases. To satisfy the numerical model, experimentally measured surface tension and contact angle values were used as references. Considering that infiltrations were studied through 5 h, utilizing static values that were achieved over the course of minutes should be acceptable. A surface tension of 0.5 N/m[20] and a contact angle between the slag and the refractory of roughly 20° at 1400°C[19] were considered. The pore size at the fluid head governs the ultimate penetration depth, so pore sizes of the virgin refractory were extracted using mercury porosimetry. Since the refractory systems exemplified a distribution of pore sizes, mean pore radii of the refractories were used. Equation (1) was used in conjunction with Factsage viscosity model.[16] The experimental and computed infiltration depths are summarized in Table III. The physical model was incapable of predicting infiltration depths for the 90%Cr_2O_3–10%Al_2O_3 since the formulation did not account for the thermodynamics and kinetics responsible in the formation of the protective layer on the top interface. The correspondence between the numerical projections and the experimental results demonstrates that changes in viscosity induced by the materials' different chemistries carried great importance in determining the infiltration depth. Although the physical model demonstrates a high degree of agreement when infiltration is driven by

Table III. Experimental and Computed Slag Infiltrations Depths

	Experimental infiltration (mm)	Computed infiltration (mm)
99%Al_2O_3	12.7	15.0
85%Al_2O_3–15%SiO_2	3.8	3.1
90%Cr_2O_3–10%Al_2O_3	N/A	N/A

N/A, Not applicable.

capillary pressures,[7] it does not encapsulate the entirety of the degradation process, including factors that influence physical and chemical spallation. Accordingly, although the 85%Al_2O_3–15%SiO_2 refractory resisted substantial slag infiltration, its effectiveness needs to be confirmed in actual gasification conditions where fresh incoming slag may constantly dissolve the matrix microstructure and spall away the aggregate materials.

In contrast to the 99%Al_2O_3 system, the 85%Al_2O_3–15%SiO_2 and 90%Cr_2O_3–10%Al_2O_3 refractories performed remarkably well by preventing slag flow into its microstructure. Interactions with the 85%Al_2O_3–15%SiO_2 refractory elevated the SiO_2 content of the slag and thereby limited infiltration with increased slag viscosities. In response to the chemistry of the coal slag, the 90%Cr_2O_3–10%Al_2O_3 refractory produced a Fe–Cr-oxide phase, which formed as an intermediary step in an attempt to reach equilibrium. The effectiveness of these processes provide clues to the possibility of using them as preventative defense mechanisms rather than as passive responses to slag. Refractories containing heightened concentrations of network-forming species can be used. Otherwise, barrier layers, based on intermediate equilibrium phases, can be proactively formed before full operation of the gasifier. A process described by the steelmaking industry as "glazing"[12,13] can be utilized. Prior to the introduction of the feedstock, a mixture of oxides that are designed to form a desired barrier phase can be applied onto the surfaces of the refractory walls. Such techniques can possibly lower consumable costs and eliminate the need for materials such as those based on Cr_2O_3, which are known to produce toxic by-products.

V. Conclusion

The infiltration properties of the synthetic coal slag into the respective refractory systems highlighted the importance of the microstructure and the chemical constituents of the aggregate and matrix materials. Interactions between the 90%Cr_2O_3–10%Al_2O_3 refractory and the slag produced a uniform layer of $FeCr_2O_4$ on the top interface and obstructed excessive slag flow into the bulk material. With the 99%Al_2O_3 and 85%Al_2O_3–15%SiO_2 systems, slag infiltrated into the refractory by preferentially consuming and flowing through the matrix regions of the refractory. The slag aggressively consumed the matrix material from the 85%Al_2O_3–15%SiO_2 system since the microstructure largely consisted of a glassy alumino-silicate phase, which was absorbed more rapidly into the slag than the fine crystalline particles found in the other two refractory varieties. As a result of consuming this glassy phase, infiltration into the 85%Al_2O_3–15%SiO_2 system yielded a higher viscosity slag and shallower penetration depth than for infiltration into the 99%Al_2O_3 system. The physical model that considered changes in slag fluid viscosity with regards to both temperature and composition projected comparable infiltration depths as those experimentally observed.

Acknowledgments

Technical support in conducting experiments by Rick Krabbe, David Boyd, David Smith, Jinichiro Nakano, Kyei-Sing Kwong at NETL, and Nathan Howell at CMU is greatly appreciated.

This technical effort was performed in support of the National Energy Technology Laboratory's ongoing research in Control of Carbon Feedstock and Impact on Gasifier under the RES contract DE-FE0004000.5.671.238.001.

References

[1]J. P. Bennett, K. S. Kwong, C. P. Dogan, and R. E. Chinn. "Improved Refractory for Slagging Gasifiers in IGCC Power Systems"; in *18th Annual Conference on Fossil Energy Materials*. DOE/ARC-2004-036, Oak Ridge National Laboratory, Knoxville, TN, Fossil Energy Program, Oak Ridge, TN, 2004.

[2]W. E. Lee and S. Zhang, "Melt Corrosion of Oxide and Oxide-Carbon Refractories," *Int. Mater. Rev.*, **44** [3] 77–104 (1999).

[3]C. A. Schacht, *Refractories Handbook*. Marcel Dekker, New York, NY, 2004.

[4]E. Blond, N. Schmitt, F. Hild, P. Blumenfeld, and J. Poirier, "Effect of Slag Impregnation on Thermal Degradations in Refractories," *J. Am. Ceram. Soc.*, **90** [1] 154–62 (2007).

[5]Z. Guo, "Refractories for Gasifiers," *Am. Ceram. Soc. Bull.*, **83** [6] 9101–8 (2004).

[6]T. K. Kaneko, J. P. Bennett, and S. Sridhar, "Effect of Temperature Gradient on Industrial Gasifier Coal Slag Infiltration into Alumina Refractory," *J. Am. Ceram. Soc.*, **94** [12] 4507–15 (2011).

[7]T. K. Kaneko, J. Zhu, H. Thomas, J. P. Bennett, and S. Sridhar, "Influence of Oxygen Partial Pressure on Synthetic Coal Slag Infiltration into Porous Al_2O_3 Refractory," *J. Am. Ceram. Soc.*, **95** [5] 1764–73 (2012).

[8]J. Matyas, S. K. Sundaram, B. J. Hicks, A. B. Edmondson, and B. M. Arrigoni, "Slag-Refractory Interaction in Slagging Coal Gasifiers," *Mater. Sci. Forum*, **595–598**, 397–405 (2008).

[9]J. Rawers, J. Kwong, and J. P. Bennett, "Characterizing Coal-Gasifier Slag/Refractory Interactions," *Mater. High Temp.*, **16** [4] 219–22 (1999).

[10]R. E. Williford, K. I. Johnson, S. K. Sundaram, and S. Pilli, "Effective Diffusivity and Spalling Models for Slagging Coal Gasifiers," *J. Am. Ceram. Soc.*, **91** [12] 4016–22 (2008).

[11]W. A. Selvig and F. H. Gibson, *Analyses of Ash from United States Coals (Volume 567 of Bulletin (United States Bureau of Mines))*. United States Government Printing Office, Washinton, DC, 1956.

[12]G. J. Browning, G. W. Bryant, H. J. Hurst, J. A. Lucas, and T. F. Wall, "An Empirical Method for the Prediction of Coal Ash Slag Viscosity," *Energy Fuels*, **17** [3] 731–7 (2003).

[13]H. J. Hurst, F. Novak, and J. H. Patterson, "Viscosity Measurements and Empirical Predictions for Some Model Gasifier Slags," *Fuel*, **78** [4] 439–44 (1999).

[14]B. J. Keene and K. C. Mills, *Slag Atlas*, 2nd edition. UK Woodhead Publishing Limited, Sawston, Cambridge, 1995.

[15]L. R. Rossi and W. G. Lawrence, "Elastic Properties of Oxide Solid Solutions: The System Al_2O_3–Cr_2O_3," *J. Am. Ceram. Soc.*, **53** [11] 604–8 (1970).

[16]C. W. Bale, P. Chartrand, S. A. Decterov, G. Eriksson, K. Hack, R. B. Mahfoud, J. Melancon, A. D. Pelton, and S. Petersen, "FactSage Thermochemical Software and Databases," *Calphad J.*, **62**, 189–228 (2002).

[17]K. C. Mills, "The Influence of Structure on the Physico-Chemical Properties of Slags," *ISIJ Int. (Jpn.)*, **33** [1] 148–55 (1993).

[18]D. R. Poirier and G. H. Geiger, *Transport Phenomena in Materials Processing*. The Minernals, Metals, and Materials Society, Warrendale, PA, 1994.

[19]H. Towers, "Contact Angle Measurements of Slags on Solid Surfaces," *Trans. J. Br. Ceram. Soc.*, **53** [3] 180–202 (1954).

[20]S. Vaisburd and D. G. Brandon, "A Combined Unit for Viscosity, Surface Tension and Density Measurements in Oxide Melts," *Meas. Sci. Technol.*, **8**, 822–6 (1997). □